Multi-Sensor NDVI Analysis of Eruption Impacts and Vegetation Recovery at Mount Kelud, East Java (2013–2025)

Bubacarr Jawla[1], Yesenia Zabrina Maharani Yaffa Hardianto[2], Omar M Camara[3], Faye Jerreh Manneh[4], Sainey Danjo[5], Sherif A Bah[6]

[1,2,3] Natural Resources and Environmental Engineering Study Program (Postgraduate), Department of Biosystem Engineering, Faculty of Agro-Industrial and Biosystems Technology, Universitas Brawijaya, Malang, Indonesia
[4] Faculty of Agriculture and Environmental Sciences, University of The Gambia, Faraba, Gambia
[5] Department of Plant Pathology, Faculty of Agriculture, Universitas Brawijaya
[6] Faculty of Mathematics and Natural Sciences (FMIPA), Universitas Brawijaya
[*)] Correspondence author's email: bubacarrjawla@student.ub.ac.id

Citation:
Bubacarr Jawla[1], Yesenia Zabrina Maharani Yaffa Hardianto[2], Faye Jerreh Manneh[3], Sherif A Bah[4], Omar M Camara[5,] and Sainey Danjo[2] (2026). *Multi-Sensor NDVI Analysis of Eruption Impacts and Vegetation Recovery at Mount Kelud, East Java (2013–2025)* . Jurnal Sains Geografi. Vol. 4, No. 1.

Article History:
Received: 26 April 2026
Revised: 10 Mei 2026
Accepted: 25 Mei 2026
Online: 1 Juni 2026
Published: 31 Mei 2026

Abstract

This study examined the effects of the February 2014 volcanic eruption of Mount Kelud, East Java, Indonesia, on vegetation dynamics and subsequent recovery using multi-temporal satellite-derived Normalized Difference Vegetation Index data. Despite extensive use of the Normalized Difference Vegetation Index in post-disaster analysis, long-term multi-sensor studies in tropical volcanic regions remained scarce. Landsat 8 Operational Land Imager and Sentinel-2 Multispectral Instrument imagery were combined to assess spatial and temporal vegetation changes from 2013 to 2025. The Normalized Difference Vegetation Index declined by more than 0.50 units immediately following the eruption, confirming significant vegetation loss from ashfall, pyroclastic flows, and lahars. Recovery was rapid, with values returning to pre-eruption levels within one year and surpassing the baseline in subsequent years (0.80–0.87). Damage classification revealed that 89% of sampled sites experienced low-severity disturbance, reflecting spatial heterogeneity in eruption impacts. Statistical analysis indicated no significant seasonal influence on Normalized Difference Vegetation Index variability, suggesting that vegetation dynamics were driven primarily by disturbance rather than climatic seasonality. These findings demonstrated that multi-sensor Normalized Difference Vegetation Index analysis effectively tracked post-eruption recovery and highlighted the resilience of tropical volcanic ecosystems.

Keywords: Normalized Difference Vegetation Index, volcanic eruption, vegetation recovery, satellite remote sensing, Mount Kelud

Abstrak

Studi ini mengkaji dampak erupsi vulkanik Gunung Kelud, Jawa Timur, Indonesia pada Februari 2014 terhadap dinamika vegetasi dan pemulihan selanjutnya menggunakan data Normalized Difference Vegetation Index (NDVI) multi-temporal yang diturunkan dari citra satelit. Meskipun NDVI telah digunakan secara luas dalam analisis pascabencana, studi multi-sensor jangka panjang di kawasan vulkanik tropis masih sangat terbatas. Citra Landsat 8 Operational Land Imager dan Sentinel-2 Multispectral Instrument digabungkan untuk menilai perubahan vegetasi secara spasial dan temporal dari tahun 2013 hingga 2025. Nilai NDVI menurun lebih dari 0,50 unit segera setelah erupsi, mengonfirmasi kehilangan vegetasi yang signifikan akibat hujan abu, aliran piroklastik, dan lahar. Pemulihan berlangsung dengan cepat, dengan nilai yang kembali ke tingkat pra-erupsi dalam satu tahun dan melampaui nilai dasar pada tahun-tahun berikutnya (0,80–0,87). Klasifikasi kerusakan menunjukkan bahwa 89% lokasi sampel mengalami gangguan dengan tingkat keparahan rendah, mencerminkan heterogenitas spasial dalam dampak erupsi. Analisis statistik menunjukkan tidak adanya pengaruh musiman yang signifikan terhadap variabilitas NDVI, mengindikasikan bahwa dinamika vegetasi lebih didorong oleh faktor gangguan daripada musiman iklim. Temuan ini menunjukkan bahwa analisis NDVI multi-sensor secara efektif dapat melacak pemulihan pascaerupsi dan menyoroti ketahanan ekosistem vulkanik tropis.

Kata kunci: Normalized Difference Vegetation Index, erupsi vulkanik, pemulihan vegetasi, penginderaan jauh satelit, Gunung Kelud

1. INTRODUCTION

Natural hazards in mountainous tropical ecosystems include volcanic eruptions and landslides, which can be extremely devastating to the ecosystem. Such occurrences may lead to a high level of destruction of vegetation cover, soil structure, and landscape stability, thus affecting the ecological balance as well as making the slope prone to other hazard events in the future (Geertsema & Pojar, 2007; Chiessi *et al*., 2010). Landscapes following disturbance experience significant physical and biological changes, such as loss of vegetation cover, bare ground, and increased erosion that decrease slope stability and increase the likelihood of future failures (Chilton & Spotila, 2020). Physical, chemical, and biological processes in an intricate interconnection control the further process of ecological recovery, and one of the keys to long-term slope recovery and ecological stability is identified with vegetation regeneration (McLean *et al*., 2021).

Regrowth of vegetation after disturbance events is one of the main indicators of the natural restoration of slope stability in mountains. Reproduction of communities of trees and

their remaining root systems is extremely important in the anchoring of soils and in lowering rates of erosion (Kong *et al*., 2025; Song *et al*., 2024; Mandl *et al*., 2026). Nevertheless, the vegetation recovery process is extremely irregular and is influenced by the intensity of the disturbance, environmental factors in that area, and biological properties of the communities of flora at the impacted location (Lancheros *et al*., 2019). Vegetation recovery in mountainous tropical areas will usually be natural, but may be much faster than in temperate areas because of maximum year-round photosynthesis due to a combination of consistently warm temperatures and high precipitation levels (Poorter *et al*., 2016a; Lusiana *et al*., 2026).

Mount Kelud is an Indonesian historic and highly destructive stratovolcano found in the East Java Province at a latitude of about 7.93°S, a longitude of about 112.31° E, at a summit elevation of about 1,731 meters above sea level (Maeno *et al*., 2019). The volcano has a long-recorded history of luminous eruptions, with the last significant eruption occurring on 13-14 February 2014. This outburst generated a considerable column of the eruption more than 17 kilometers in height and caused the deposition of large amounts of volcanic ash, tephra, and pyroclastic material against the landscape of the area, with virtually all vegetation cover being destroyed on the upper and mid-slope of the mountain (Suzuki & Iguchi, 2019). The 2014 outburst was then followed by the lahar action and the second mass movement, resulting in various landslide scars, further distorting the conditions of soil and vegetation on the covered territory (Global Volcanism Program, 2014).

Remote sensing technology has emerged as the most viable method of tracking vegetation recovery of large spatial areas and longer periods in remote mountainous areas (Patera *et al*., 2026). One of the most popular spectral indices used in estimating vegetation density, health, and productivity with the help of satellite images is the Normalized Difference Vegetation Index (NDVI), which is based on the near-infrared and red band reflectance ratio (Tucker, 1979a; Huete *et al*., 2002a). NDVI has been widely used in post-disturbance vegetation recovery research, such as landslides, wildfires, and volcanic eruptions, and is a useful proxy to monitor slow vegetation recovery (biomass and canopy cover) over time (Tucker, 1979b; Verbesselt, Hyndman, Zeileis, *et al*., 2010; Plank *et al*., 2016). However, NDVI is widely used in post-disturbance research; the long-term vegetation recovery of volcano-disturbed areas in tropical environments remains insufficiently understood. Existing research often relies on short-term or single-sensor analyses, with limited focus on Mount Kelud and a lack of integrated multi-sensor approaches.

This study integrates data from two complementary satellite platforms: (1) multi-temporal Landsat 8 OLI imagery (30 m spatial resolution, 16-day revisit cycle) covering the period 2013–2015; and (2) Sentinel-2 MSI imagery, which provides higher temporal frequency and finer spatial resolution for NDVI monitoring and detailed damage classification over 100 sample locations from 2015 to 2025. The integration of these datasets enables a multi-scale and comprehensive assessment of post-eruption vegetation dynamics at Mount Kelud, improving both temporal continuity and spatial detail of vegetation recovery analysis.

Therefore, the objectives of this study are: (I) to quantify the temporal trajectory of vegetation recovery at eruption-disturbed and landslide-affected areas on the flanks of Mount Kelud using multi-temporal NDVI data; (II) to evaluate the spatial distribution and severity of eruption damage through NDVI anomaly analysis; and (III) to examine the influence of seasonal patterns and topographic factors on vegetation recovery variability.

2. METHOD

This section outlines the data collection process, data processing, and analysis process, including the process of acquiring satellite data, calculating NDVI, classification of seasons, and the statistical methods of data analysis.

2.1 Study Area

Mount Kelud is a volcanic mountain, a stratovolcano, in the East Java Province, Indonesia, at around 7.93°S and 112.31°E (**Figure 1**). The volcano lies at an elevation of about 1,731 metres above sea level and is located 27 kilometres northeast of Kediri and 56 kilometres southwest of Malang. The area of the study deals with the volcanic slopes and the immediate surroundings of the eruption and the mass movements which followed the 2014 eruption, and the area covered the boundaries of Kediri, Blitar, and Malang Regencies. The topography of the landslides and disturbance in this study was mostly located in the range of 700-1700 above sea level, with slopes of 5°C to above 40°C, most commonly southward, southeastern, and eastern.

The climate of the Mount Kelud area is of a tropical monsoon type, and there are two seasons. The wet season lasts between October and April (some classifications have it as November through April), with about 200 mm of precipitation per month during the peak months, and the dry season is May to September/October with less but not negligible rainfall. In the region under study, rainfall per annum averages between 1,800 and 2,500 mm, with the highest amounts found at higher elevations owing to the orographic boost. The average temperature is 18°C to 28°C at the study sites, and the values are always above 20°C over the year at the mid-slope level. These desirable thermal and humidity regimes are predicted to maintain the nature of year-round photosynthesis as well as to promote a relatively fast post-disturbance recovery of vegetation.

Andesitic and dacitic volcanic products, which comprise lava flows, pyroclastic deposits, and volcanic breccias, are the dominant products that form the geology of Mount Kelud and are formed because of the repetitive eruptive cycles. The soils formed on these volcanic materials are mostly Andisols and Inceptisols, which are highly porous, have good water retention, and have a relatively high natural fertility due to the constant deposits of volcanic ash and minerals. The vegetation distribution is also elevational with a zonation typical of Javan stratovolcanoes, with lower elevation areas having agricultural land and plantation cover, which give way to a mixed montane forest (Pinus merkusii, Casuarina junghuhniana) to the mid-elevations and finally ericaceous scrub at the upper montane zone.

In 2014, the eruption of Mount Kelud (Volcanic Explosivity Index = 4) produced 50-100 million cubic meters of volcanic material, which was distributed over a radius of up to 500 kilometers, with the worst vegetative damage occurring in a 10-kilometer radius of the summit. In the study area, eruption products such as tephra, pyroclastic density currents, and ballistic ejecta had nearly destroyed the vegetation on the upper and mid flanks of the volcano. Lahar flows, and secondary landslides then continued to disorder the vegetation and soils on the lower slope, offering a model of the severity of disturbance and levels of recovery following disturbance.

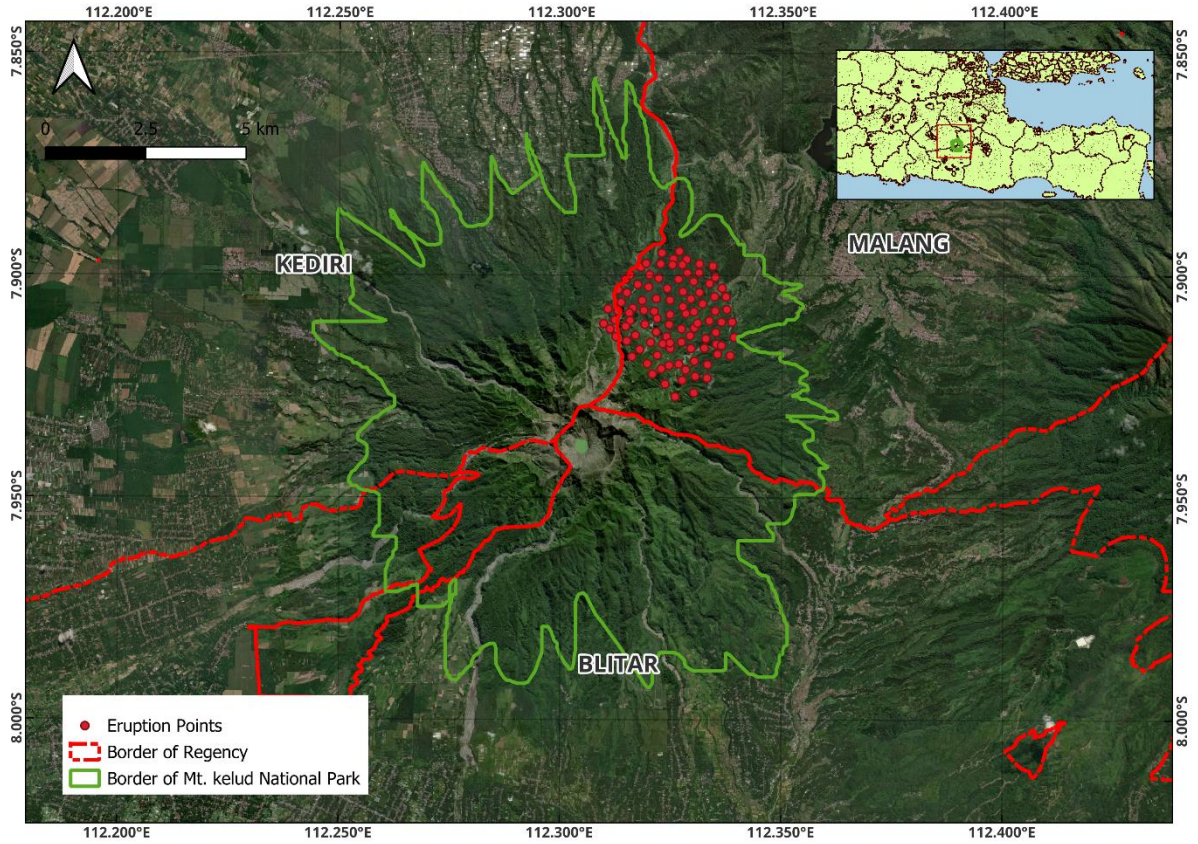

Figure 1. Presents the spatial distribution of eruption-related observation points around Mount Kelud, East Java, Indonesia

2.2 Multi-Sensor Satellite Data

In this study, a multi-sensor approach is adopted to provide coverage of the entire 2013-2025 study period, based on the availability of the satellite platforms. From 2013 to 2015, before the launch of Sentinel-2 (in June 2015), NDVI monitoring was based solely on Landsat 8 OLI (Operational Land Imager) Level 2 surface reflectance data downloaded via USGS Earth Explorer (https://earthexplorer.usgs.gov/). 2015 onwards, Sentinel-2 MSI is combined with Landsat 8 using the Harmonized Landsat and Sentinel-2 (HLS) approach (Claverie et al., 2018b) to provide more frequent and higher-resolution data. This approach provides full temporal coverage of the pre-eruption baseline (2013), the eruption event (2014), and the entire multi-year recovery period (2015-2025) and cross-calibrates the records of the two sensors in the overlapping years (2015-2025) to ensure congruence in NDVI trends. In total, 102 images were initially obtained between 2013 and 2025; after cloud screening (no more than 10% cloud cover), a quality-controlled temporal subset was obtained. Band 4 (Red, 0.64–0.67 µm) and Band 5 (NIR, 0.85–0.88 µm) at 30 m spatial resolution were used to compute NDVI (as shown in **Table 1**). The USGS scaling factor of 0.0000275 with an additive offset of -0.2 was used to convert all digital number values to surface reflectance (Landsat Collection 2 Level 2 convention). For the Sentinel-2 MSI, Band 4 (Red, 0.65-0.68 µm) and Band 8 (NIR, 0.84-0.88 µm) with 10 m resolution were used for the calculation of NDVI (see **Table 1**), with surface reflectance data downloaded from the Copernicus Open Access Hub as Level-2A (Bottom-of-Atmosphere) products, and therefore no additional atmospheric correction was necessary.

Table 1. Presents satellite sensors and spectral bands used for NDVI calculation

Sensor	Band	Wavelength (μm)	Usage
Landsat 8 OLI	Band 4 (Red)	0.64–0.67	Red reflectance for NDVI calculation
Landsat 8 OLI	Band 5 (NIR)	0.85–0.88	NIR reflectance for NDVI calculation
Sentinel-2 MSI	Band 4 (Red)	0.65–0.68	10 m
Sentinel-2 MSI	Band 8 (NIR)	0.84–0.88	10 m

2.3 NDVI Calculation and Quality Screening

The Standard formula used to compute the Normalized Difference Vegetation Index (NDVI) was used to measure vegetation conditions at each observation point based on satellite surface reflectance imagery:

$$NDVI = (NIR - Red) / (NIR + Red) = (Band\ 5 - Band\ 4) / (Band\ 5 + Band\ 4) \quad (1)$$

The values of NDVI are between -1 and +1, with more positive values suggesting denser and healthier vegetation cover. Areas of bare soil, volcanic base, or sparse vegetation tend to have NDVI values less than 0.3, and dense montane forest cover will have values of 0.6 to 0.9. The conversion of the surface reflectance to Landsat 8 was done using:

$$SR = DN \times 0.0000275 - 0.2 \quad (2)$$

The original pool of Landsat images was subjected to a quality screening procedure. Pearson correlation ($p < 0.05$) was performed between adjacent image dates at randomly selected stable vegetation pixels to determine images with anomalous NDVI values. Annual maximum NDVI is used to reduce the phenological variability between seasons and enable recovery trends to be assessed without considering within-year variability. All processes were conducted using the latest version of QGIS (version 3.44.7-Solothurn).

2.4 Seasonal Classification

Indonesia has a tropical climate regime, and seasons were categorized using it. In Landsat 8, the growing season was identified as the period between October and March, and the non-growing season was between April and September. Having two seasons (wet and dry) is used when reporting on Sentinel-2 analysis: November-April is considered the wet season, and May-October is dry. This was the same classification that was used throughout the years to carry out analysis of the trend, statistical test, and inter-seasonal correlation.

2.5 Eruption Damage Classification

To evaluate the impact of the eruption, a per-location baseline NDVI was computed as the average value of all the pre-eruption values (Sentinel-2 database). An NDVI anomaly was further determined during the period of the eruption (February 1 to June 30, 2014), and each sample was classified by the highest level of damage severity (as shown in **Table 2**):

Table 2. Records eruption damage classification

Damage Class	NDVI Anomaly Threshold
Severe	< -0.5
Moderate	-0.5 to -0.3
Low	-0.3 to -0.1
Minimal	> -0.1

2.6 Statistical Analysis

Both datasets were subjected to statistical analysis to determine the effects of varying seasons on the dynamics of NDVI. In the case of Landsat 8, Pearson correlation analysis and independent-samples t test were utilized to compare growing and non-growing season NDVI values. In the case of the Sentinel-2 dataset, inter-seasonal Pearson correlations between wet-season and dry-season values of NDVIs were calculated, with the years (2022, 2023, 2024) having paired observations only. Topographic controls (elevation, slope gradient, aspect) were assessed using the decision tree analysis, considering statistical splits at $p < 0.05$ with a minimum node size of 20 observations. All analyses were conducted in Python (Version 3.11.7) using SciPy and pandas libraries.

Pearson Correlation Coefficient (r)

$$r = \frac{\sum(x_i-\bar{x})(y_i-\bar{y})}{\sqrt{\sum(x_i-\bar{x})^2 \cdot \sum(y_i-\bar{y})^2}} \quad (3)$$

Or equivalently:

$$r = \frac{n\sum x_i y_i - \sum x_i \sum y_i}{\sqrt{[n\sum x_i^2 - (\sum x_i)^2][n\sum y_i^2 - (\sum y_i)^2]}} \quad (4)$$

Where:

x_i, y_i = paired NDVI observations (e.g., growing vs. non-growing season)

$\bar{x}, \bar{y}$ = respective means

n = number of observations

Independent-Samples t-test

$$t = \frac{\bar{X}_1 - \bar{X}_2}{\sqrt{\frac{s_1^2}{n_1} + \frac{s_2^2}{n_2}}} \qquad (5)$$

Where:

x ¯_1, x ¯_2 = mean NDVI for growing and non-growing seasons
s_1^2, s_2^2 = variances of each group
n_1, n_2 = sample sizes of each group

Decision Tree Split Criterion (Gini Impurity)

$$Gini = 1 - \sum_{k=1}^{K} p_k^2 \qquad (6)$$

Where:

p_k = proportion of observations belonging to class kat at a given node
K = total number of classes

3. RESULTS AND DISCUSSION

3.1. RESULTS

This section details the findings of multi-sensor NDVI analysis of the eruption's impact and vegetation recovery at Mount Kelud (2014-2025). Results are described in text, numbered tables (Tables 3-5) and numbered figures (Figures 2-8), which are all cited in the text.

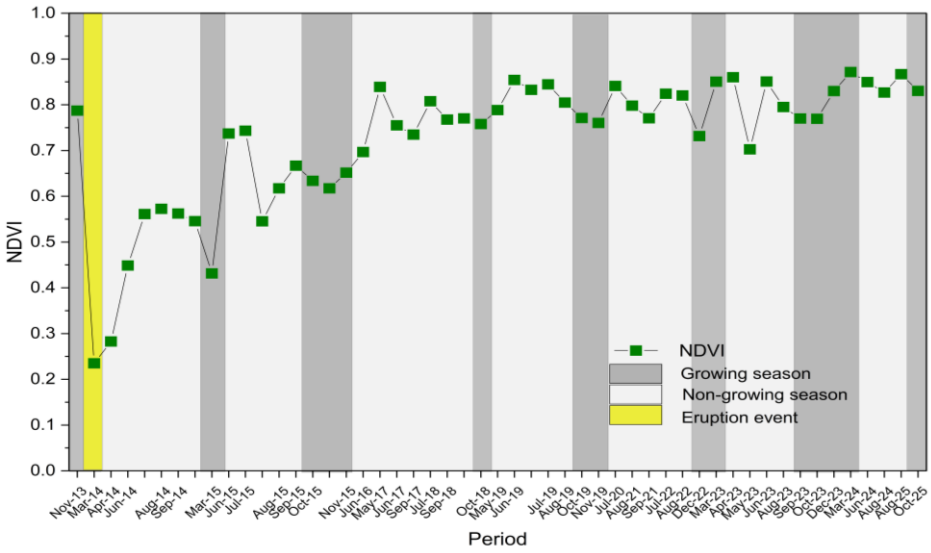

Figure 2. Presents the NDVI trends at mt. Kelud between November 2013 and October 2025 derived from Landsat 8 imagery. The growing season extends from October to March, whereas the non-growing season spans April to September

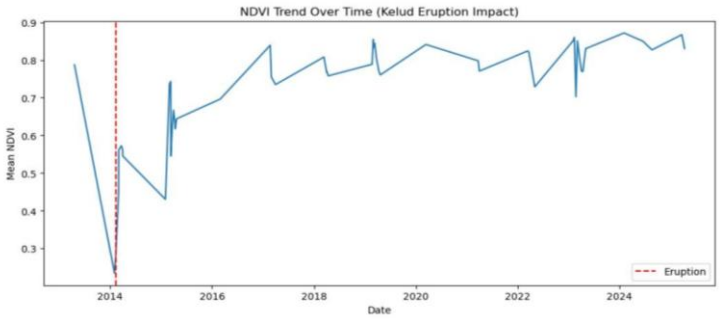

Figure 3. Shows the mean NDVI trend over time for 100 sample locations around Mount Kelud (2013–2025) derived from Sentinel-2 imagery. The red dashed vertical line marks the February 13, 2014, eruption date. The sharp post-eruption decline and subsequent multi-year recovery are clear.

3.1.1 Effects of Eruption Assessment and Classification of Damage

It was determined by analyzing NDVI anomalies of the eruption damage spatial distribution over the 100 sample sites being tracked in the Sentinel-2 dataset. The highest NDVI minimum of the time frame of the eruption (February 1 -June 30, 2014) was computed under four categories of damage as outlined in Section 3.4. The findings reveal that 89% of the tested sites were under the low level of NDVI depression (-0.1 to -0.3) and 10% were moderately damaged (-0.3 to -0.5), as shown in **Table 3**. None of the locations had severe damage (< 0.5), and only one location (1%) reported minimum impact.

Table 3. Outlines the spatial distribution of eruption damage across 100 sample locations

Damage Class	Number of Locations	Percentage (%)
Minimal (> -0.1)	1	1.0%
Low (-0.1 to -0.3)	89	89.0%
Moderate (-0.3 to -0.5)	10	10.0%
Severe (< -0.5)	0	0.0%

This distribution is probably due to a spatial gradient of the ashfall deposition over the Centre of the eruption, and the high pre-eruption NDVI baseline of the tropical thick vegetation also compacted to limit the amount of additional anomaly that could have been achieved. The fact that the sample of 100 points did not have any severe instances of damage class (NDVI anomaly < -0.5) can also suggest that the heterogeneous disturbance mosaic was sampled, as opposed to the most directly adjacent and severely affected areas.

3.1.2 Post-Eruption Vegetation Recovery Trajectory

The recovery analysis after the eruption consistently shows a definite and persistent positive trend in the average NDVI in both sensor sequences. From a post-eruption minimum of approximately 0.23–0.28 Landsat 8 in mid-2014, mean NDVI rose to the 0.65–0.75 range by late 2014 to early 2015. According to the Landsat 8 dataset, NDVI values have gone down to

almost pre-disturbance levels of 0.70-0.75 in about one year after the eruption and then remained at the same level, slightly higher than pre-disturbance values, which are 0.80-0.87.

This fast growth rate is also in line with the good climate factors at Mount Kelud, whereby the warm temperature of more than 20°C throughout the year and the average rainfall of 1,800 to 2,500 mm provide a year-round growing environment, and the richness of Andisol soils resulting from the volcanic ash deposits.

3.1.3 Seasonal Analysis

3.1.1.1 Pearson Correlation Test

The PEARSON correlation test was used to test the relationship between the NDVI values and their seasonal classification (growing and non-growing season), resulting in a correlation coefficient of r =0.095 and a p-value of 0.506 (>0.05) as shown in **Table 4**. The small correlation coefficient of the variable NDVI and season shows that there is no meaningful linear relationship between these two variables, whereas the insignificance of the p-value proves the fact that the latter does not achieve the desired level of statistical significance of 0.05. This result shows that the seasonal monsoon cycle is not statistically significant in affecting NDVI variability of the Landsat 8 data.

Table 4. Indicates Pearson correlation test (Landsat 8 dataset, n = 51)

		NDVI	**Season code**
NDVI	Pearson Corr.	1	-0.09536
	p-value	--	0.50562
Season code	Pearson Corr.	-0.09536	1
	p-value	0.50562	--

3.1.1.2 The Independent Sample T-test (Landsat 8)

The independent samples t-test of mean NDVI in growing season (n=15, mean=0.702, SD=0.172) and non-growing season (n=36, mean=0.732, SD=0.134) produced a t-test= -0.606 with 21.49 degrees of freedom and a p-value=0.55 (as shown in **Table 5**). The average difference of -0.030 is negligibly small considering the range of NDVI. The fact that NDVI had a slight mean difference during the non-growing period (dry season) than during the growing period (wet season) could be attributed to the circumstance that more occasions were recorded when there was no cloud, and the results were closer to the true picture of the vegetation greenness.

Table 5. Highlights descriptive statistics by season (Landsat 8)

		N	**Mean**	**SD**	**SEM**	**Median**
1	Growing season	15	0.70186	0.17185	0.04437	0.76031
0	Non-growing season	36	0.73197	0.13442	0.0224	0.77025
	Difference		-0.03011		0.0449	
	Overall	51	0.72312	0.14529	0.02035	0.76993

T-test: t = −0.606, df = 21.49, p = 0.551 (not significant)

3.1.1.3 Seasonal mean NDVI and Distribution (Sentinel-2)

The seasonal mean NDVI values obtained over the entire Sentinel-2 observation period from 2013 to 2025 reveal that the dry season has a mean of 0.809, slightly greater than the wet season mean of 0.716 (as apparent in **Figure 4**). Such a counterintuitive outcome is mainly due to the dataset's temporal composition: the 2014 eruption occurred in the wet season (February), and the subsequent disastrous decrease in NDVI strongly reduces the wet-season average, as observed in **Figure 5**. However, during eruption-free years, both seasons still have high NDVI (>0.75), indicating the perennial green vegetation cover of the Kelud highland area. All these findings in the Sentinel-2 dataset are entirely in agreement with those of Landsat 8, and collectively, they allow finding that there is no important control of seasonal NDVI using both systems.

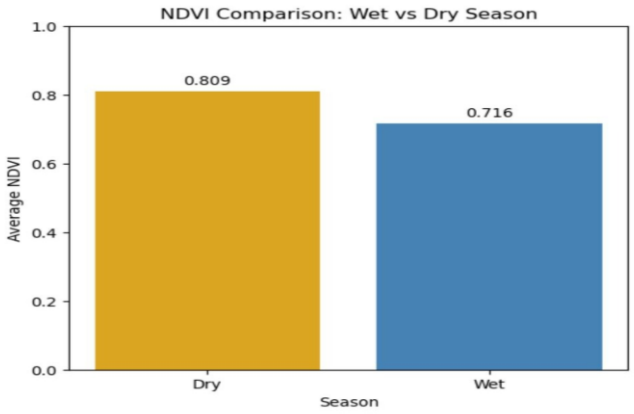

Figure 4. Shows bar chart comparing mean ndvi values between the dry season and wet season across all years (2013–2025, sentinel-2). the lower wet season is primarily driven by the february 2014 eruption impact.

3.1.1.4 Overall NDVI Temporal Trend (2013–2025)

The temporal NDVI trend analysis showed that the vegetation cover in the study area was significantly and dramatically changed by the February 2014 eruption, as depicted in **Figures 2 and 3**. Before the eruption, the mean NDVI levels were high, with mean values of about 0.75-0.88 in both sensor systems between sample points on the slopes of the mountain Kelud, which showed that dense and healthy vegetation was present on the slope of the mountain. After the eruption on the 13th of February 2014, there were sharp declines in the mean NDVI values. Volcanic ash fall, lahar, and pyroclastic deposition are also known to have a destructive impact, and the Landsat 8 dataset showed a loss of over 0.50 NDVI units between pre-disturbance values of around 0.75-0.80 and post-eruption values of 0.23-0.28.

Subsequent years revealed that, in the years after the eruption, the NDVI values at disturbed sites gradually rose, which was because of the re-establishment of pioneer and secondary vegetation on the volcanic substrate. The values also were stable between 0.80 and 0.87 in 2020-2025 in both data sets, indicating a significant recovery of the ecosystem. The occurrence of periodic drops on the post-2019 signal could be indicative of secondary disturbances like lahars, land use change, or seasonal drought stress.

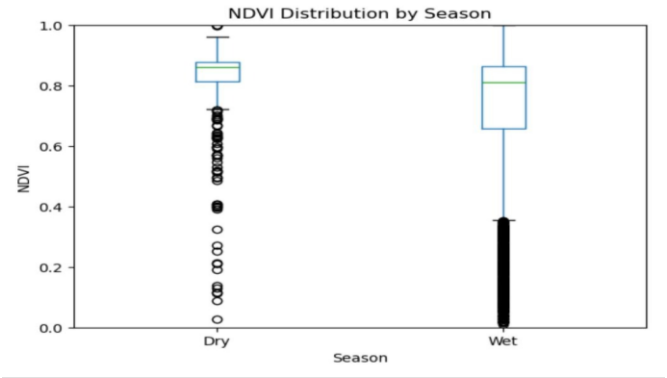

Figure 5. Presents a boxplot showing NDVI distribution by season (Sentinel-2). The wider range and lower outliers in the wet season distribution reflect the concentrated eruption impact in February 2014, which falls within the wet season.

3.1.1.5 Monthly NDVI Pattern

The bimodal pattern of seasonality of the NDVI monthly pattern, calculated as an average of all Sentinel-2 measurements recorded in each calendar month, indicates a seasonal distribution. January has the greatest average per month (~0.85) with a sharp decline in February (~0.64), which can be solely attributed to the 2014 eruption. There was a secondary peak in June-August (~0.85), which was in the dry season, as displayed in **Figure 6**. Without the February 2014 eruption alert, perhaps the trend would indicate a slower transition between wet and dry periods, with a slight seasonal change characteristic of tropical evergreen plants. The February outlier highlights the importance of large disturbance events dominating multi-year averages monthly.

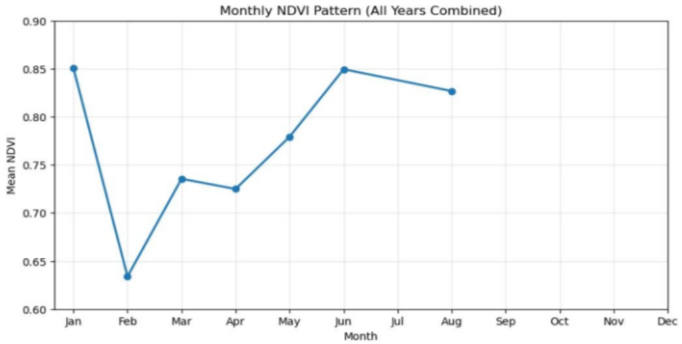

Figure 6. Presents monthly means of the NDVI pattern (all years combined, Sentinel-2). The sharp trough in February reflects the 2014 eruption's impact. The bimodal pattern shows high greenness in both January and June–August, with mid-year stability in the dry season.

3.1.1.6 Inter-Seasonal NDVI Correlation (Sentinel-2)

Pearson correlation was used to compare the values of wet-season and dry-season NDVI of the same year (paired observations): 2022, 2023, and 2024. The correlation coefficient increased progressively from r = 0.257 in 2022 to r = 0.756 in 2023 and r = 0.582 in 2024 (as illustrated in **Figure 7**). The weak correlation in 2022 indicates spatial heterogeneity in the current recovery; other parts of the habitat had recovered more quickly than others, breaking the co-variation of wet/dry that should occur in a mature stable canopy. The trend of strengthening implies that the regaining vegetation is nearing a similar structure whereby the relative

greenness of a location remains constant over seasons, showing progressive convergence towards a steady state of the ecosystem.

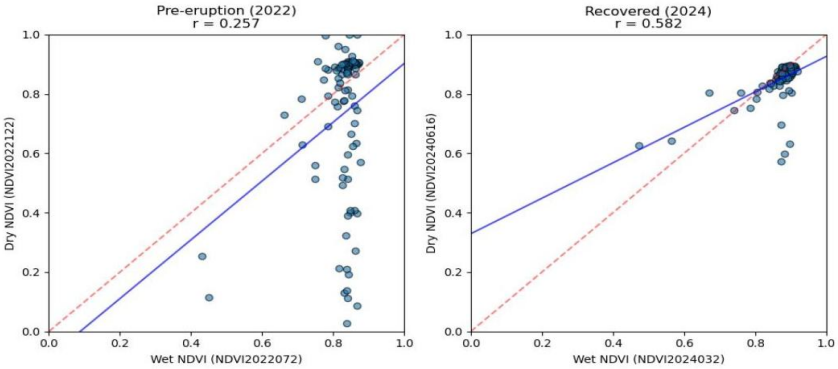

Figure 7. Illustrates scatter plots of wet-season vs. dry-season NDVI for 2022 (left, r = 0.257) and 2024 (right, r = 0.582). The strengthening correlation indicates increasing spatial coherence in vegetation structure as the landscape continues to recover.

3.1.1.7 Annual Wet vs. Dry Season NDVI Trajectory

Mean NDVI by season, annual breakdown, is a clear representation of the course of eruption impact through recovery. In 2013, there were only wet-season Sentinel-2 data with a mean of approximately 0.79. The eruption year 2014 has the smallest wet season mean (~0.47), which is the largest disturbance signal. Since 2015, the values of wet and dry season NDVI have progressively risen, with data on dry seasons becoming available since 2022. The means of dry and wet seasons are very similar in 2023-2024 (both near 0.83-0.88), indicating a relatively stable and steady seasonal recovery of vegetation, as demonstrated in **Figure 8**. This seasonal accumulation of NDVI across years aligns with long-term recovery patterns in the Landsat 8 data and indicates the gradual restoration of a mature, resilient vegetation canopy.

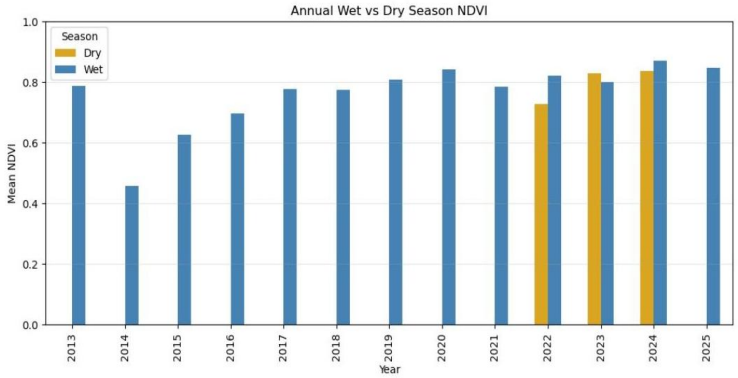

Figure 8. Shows annual means of NDVI by season (wet = blue, dry = goldenrod) from 2013 to 2025 (Sentinel-2). The 2014 eruption shows the lowest wet season NDVI, followed by a steady multi-year recovery. Dry season data from 2022 onward track closely with wet-season values, indicating a recovering and increasingly stable ecosystem.

3.2 DISCUSSION

This section discusses the study's findings against existing literature on vegetation recovery after volcanic eruptions, NDVI remote sensing, and tropical ecosystems, in themed sub-sections covering vegetation loss from eruptions (Section 3.1.1), rapid recovery (Section 3.1.2), seasonal NDVI changes (Section 3.1.3), coherence of NDVI across seasons (Section 3.1.4), and implications and limitations for vegetation monitoring (Section 3.1.5).

3.2.1 Magnitude and Spatial Pattern of Eruption-Induced Vegetation Loss

NDVI fell by at least 0.50 units following the eruption of Mount Kelud in February 2014, which is comparable to the vegetation damage reported at other similar locations of tropical volcanic disturbances. Similarly, deep depressions of NDVI after pyroclastic and lahar events that occur at active Indonesian volcanoes were recorded by Rösch, M., & Plank, S. (2022), Furusawa *et al*. (2023a), and Saito *et al*. (2022), illustrating the same depressions at Aso Volcano in Japan, where NDVI was indistinguishably lower than 0.30 in the most severely impacted areas. The current investigation further develops them by offering a multi-sensor spatial view with a numeric pattern on a sample network of 100 points used to cover a wide elevational range of 700 to 1,700 above sea level.

The result of the damage classification, whereby 89% of the sample locations registered low-severity NDVI anomalies (−0.1 to −0.3) and just 10% of registered moderate anomalies (−0.3 to -0.5), with none recorded as severe (less than -0.5), has reflected the heterogeneous distribution of eruption impact across the study area. Two major factors can be attributed to this result. To begin with, the spatial sampling approach quantified a gradient of distances to the summit vent, thus combining the highly perturbed nearer zones as well as more moderately affected distal flanks into a single dataset. Second, the pre-eruption vegetation at the mid and upper slopes of the mountain Kelud was relatively dense and high-biomass forest communities (Pinus merkusii, Casuarina junghuhniana, and related undergrowth), which offer pre-eruption NDVI values in the range of 0.75-0.88. The high baseline squashes the maximum possible NDVI range: even on a location where ashfall had led to virtual canopy defoliation, the after eruption NDVI values could never drop below the reflectance floor of the underlying volcano substrate (around 0.10-0.20), and thus limited the magnitude of the anomalies and the fraction of sites that could have been classified as extremely affected. It is a constraint of the NDVI-based disturbance measurement, a phenomenon that has long been observed to happen in dense forest-covered lands with high NDVIs due to index saturation (Huang *et al*., 2021; Zheng *et al*., 2023; Gao *et al*., 2023).

The lack of severe damage categories in the current data does not, therefore, mean vegetation damage was generally mild; instead, it is a consequence of the analysis limitations of depending on an anomaly thresholding with a high tropical background. Future studies could also utilize additions to the NDVI anomaly method with other spectral measures, such as the Normalized Burn Ratio (NBR) or the Soil-Adjusted Vegetation Index (SAVI), which lessen the effects of the canopy background and potentially enhance the ability to distinguish between high backgrounds of severe damage in densely grown tropical environments.

3.2.2 Rapidity of Post-Eruption Vegetation Recovery: Climatic and Edaphic Drivers

Perhaps one of the most notable results of this research is the incredibly fast rate of vegetation recovery following an eruption event of Mount Kelud as compared to similar disturbance locations across the world. Landsat 8 shows a restoration of approximately one-year post-eruption NDVI values (0.70-0.75) with the values then stabilizing around 0.80-0.87 by 2020 to 2025. This is much more rapid than recovery intervals recorded in other volcanic and seismically disturbed tropical and subtropical locales, such as about 6 years at Mount Rinjani, Indonesia (Lusiana *et al*., 2026), 2.3-10.2 years at Tsengwen in Taiwan (Wu, 2021a), about 12 years at Aso Volcano in Japan (Saito *et al*., 2022b), and 18–20 years at Longmen Shan in China (Zhong *et al*., 2021).

The positive abiotic conditions convergence of three conditions convincingly constitutes the accelerated recovery trajectory found in Mount Kelud. Initially, the tropical climate of East Java maintains a year-round photosynthetic (warm temperatures of 18-28°C at the study sites, but staying above 20°C at the elevation of the mid-slope sites all year round) and high average annual rainfall (1800- 2500 mm), which removes the seasonal growth inactivity that limits recovery rates at temperate sites (Poorter *et al*., 2016b; Wu, 2021b).

Subsequently, the volcanic roots of Mount Kelud can largely be grouped as Andisols and Inceptisols that are a result of andesitic to dacitic origin. Andisols are also considered to be one of the most productive soils in the world in terms of agriculture and ecological activity due to their high porosity, good water holding capacity, and the constant replenishment of new volcanic minerals that ensure that the soil remains highly fertile in nature (Sundha *et al*., 2020; Dahlgren *et al*., 2004). The arrival of new tephra during and after the 2014 eruption was therefore at once a critical disturbance on the surface and the injection of mineral-rich substrate, which in turn enabled such explosive plant development and biomass growth after pioneer colonization had started. Finally, the topography of Mount Kelud, being part of the Indonesian archipelago, also means a rich regional seed pool necessary to passively spread pioneer species into disturbed regions rapidly.

It has been observed that nitrogen-fixing pioneer trees, including Parasponia rigida, have rapidly increased at volcanic substrates between 600 and 1700 meters above sea level, within the exact range of the study area. Three years after eruption, the root nodules of this species were observed to grow in individuals up to 3-10 cm in stem diameter, and 93% of the root nodules were found to be biologically active, documenting the efficiency of symbiotic nitrogen fixation in promoting pioneer biomass growth on the nutrient-poor fresh tephra (Ishaq *et al*., 2020). This swift expansion of such nitrogen-fixing trailblazer communities is compatible with the NDVI overshoot of values above pre-disturbance values of the current dataset by 2020-2025 (0.80 for 2025, marginally above the pre-disturbance range 0.7588).
This post-disturbance NDVI overshoot (as the result of the proliferation of fast-growing, high-canopy-density pioneer species on fertile Andisol substrates) is expected to be a temporary stage before re-establishing a more structurally complex mature forest canopy, and is consistent with the successional dynamics recorded in similar post-disturbance volcanic successions (Lai *et al*., 2022; Ishaq *et al*., 2020)

3.2.3 Absence of Significant Seasonal Control on NDVI Variability

The statistical results obtained from both the Landsat 8 and Sentinel-2 datasets indicate that there is no statistically significant seasonal control element affecting vegetation greenness at Mount Kelud. The Pearson correlation involving NDVI and seasonal classification in the Landsat dataset provided a non-significant coefficient of correlation ($r = -0.095$, $p = 0.506$), and the independent-samples t-test showed that there was no significant difference in the mean NDVI of growing and non-growing seasons ($t = -0.606$, $df = 21.49$, $p =$ The Sentinel-2 dataset yielded steady results, where the apparent difference between wet-season (mean = 0.716) and dry-season (mean = 0.809) means can be explained by the fact that the wet-season mean is depressed by the eruption in February 2014 and not due to actual phenological seasonality.
The results are consistent with existing knowledge of equatorial tropical ecosystems, which are characterized as largely evergreen systems with little phenological seasonality. Under these conditions, photosynthesis can be year-round as the temperature is always high, and the moisture supply is usually adequate, so seasonal changes in vegetation indices like NDVI are minimal. Empirical evidence in tropical areas, such as Southeast Asia, indicates that the variability of NDVI is not well associated with seasonal changes but rather with disturbance and interannual climate variability (e.g., El NiñoSouthern Oscillation events).

As demonstrated by Black *et al*. (2016) and Furusawa *et al*. (2023b), Southeast Asian vegetation activity has comparatively steady patterns of NDVI among seasons, and precipitation variability only has a secondary effect in non-extreme conditions. Equally, Zhu *et al*. (2016) and Chen *et al*. (2019) asserted that tropical vegetation greenness changes are more sensitive to long-term environmental change than to usual seasonal forcing. More recently, Zhang *et al*. (2023) have shown that the process of NDVI dynamics in Indonesia is

dominated by more unpredictable disturbance regimes and slowing climatic changes instead of seasonal cycles.

Accordingly, the lack of a strong seasonal NDVI on Mount Kelud is not abnormal but more of the general ecological and climatic nature of the tropical montane system in Java. In a standard case, seasonal precipitation distributions do not provide a sufficiently strong or spatially consistent condition in vegetation productivity to provide statistically significant NDVI variation on a landscape scale. Alternatively, episodic events, like volcanic eruptions, are highlighted as the main factors influencing the variability of vegetation in the study region. Slightly higher dry-season NDVI values in the Sentinel-2 data are likely due to methodological bias rather than true seasonal vegetation changes. During dry seasons, there is higher-quality data due to increased visibility, and frequent wet-season cloud cover can cause NDVI values to be artificially lower. This simply indicates that apparent seasonal differences in the tropical areas can only be interpreted as an element of optical remote sensing (Shin *et al*., 2023; Y. Chen *et al*., 2024). Future research employing cloud-penetrating techniques like SAR could give more decisive measurements. In general, vegetation variability in Mount Kelud is caused more by disturbances than by seasonal influences.

3.2.4 Progressive Stabilization Inferred from Inter-Seasonal NDVI Coherence

The increase in the inter-seasonal Pearson correlation of wet- and dry-season NDVI, peaking at r = 0.756 in 2023 and being relatively strong at r = 0.582 in 2024, demonstrates the strong effect of progressive vegetation stabilization at Mount Kelud. During the initial phases of post-eruption recovery, vegetation regrowth spatial heterogeneity, which is determined by the differences in microtopography, substrate conditions, and propagule presence, causes weak seasonal patterns in NDVI. Regions where pioneer species are actively colonized are always characterized by a higher level of NDVI, whereas underdeveloped areas have values lower in value and higher seasonality.

With the progression of the ecological succession, vegetation structure becomes more homogenous, and the spatial coherence of wet- and dry-season NDVI enhances. This trend aligns with the post-disturbance recovery process, where NDVI-based studies indicate a shift in the spatial heterogeneity to a growing structural coherence as vegetation reestablishes itself (Nguyen *et al*., 2018). Time series methods which break NDVI down into trend and seasonal components have demonstrated that these changes in spectral trajectory can be associated with specific successional stages, with dry- and wet-season signals merging as canopy structure matures (Verbesselt *et al*., 2010; Berveglieri *et al*., 2021). These trends indicate the progressive overpowering of local successional variability by common climatic controls

The fact that the correlation decreased slightly between 2023 (r = 0.756) and 2024 (r = 0.582) implies the non-linear nature of the recovery pattern, and it might have been affected by the secondary disturbances. Possible drivers are localized geomorphic processes, like lahar processes, land-use stresses in low-lying regions, and interannual climatic variability linked with the El Niño Southern Oscillation (ENSO). Interannual ENSO variability has been demonstrated to have extensive effects on vegetation productivity in tropical areas, such as Southeast Asia, where El Niño events can inhibit NDVI and create spatial variations in vegetation response (Qian *et al*., 2019; Ichii *et al*., 2002; Nagai *et al*., 2007; Jin *et al*., 2025; Arjasakusuma *et al*., 2025).

Despite this short-term decrease in spatial coherence, converging values of wet- and dry-season mean NDVI towards consistently high levels (0.83 -0.88) by 2023-2024 suggest that overall vegetation recovery is still at an advanced stage. The variability observed is thus more probably due to local disturbance patches than a reversal of the larger pattern of recovery. Comprehensively, the growing inter-seasonal coherence of NDVI is consistent with understanding that the Mount Kelud landscape is shifting in early-successional heterogeneity

to a more stable and structurally homogenous vegetation system, in line with existing paradigms of tropical ecosystem recovery after significant disturbance events.

3.2.5 Implications for Satellite-Based Post-Disaster Monitoring and Limitations

The simulation of multi-temporal Landsat 8 and Sentinel-2 NDVI time series illustrated their efficiency in operational terms of post-volcanic vegetation monitoring at the landscape. These complementary sensor properties, Landsat 8 radiometric consistency, long historical record, 30 m resolution, and Sentinel-2 increased spatial resolution (10 m) and reduced revisit frequency allowed a multi-scale evaluation of both long-term recovery patterns and fine-scale spatial heterogeneity in disturbance and regeneration processes. This multi-sensor fusion approach is consistent with the model of Harmonized Landsat and Sentinel-2 (HLS) as proposed by Claverie *et al*. (2018a) and has been gradually proven as a best practice in the ecological post-disturbance monitoring of terrain with limited field coverage (Cardille *et al*., 2022; Wulder *et al*., 2022).

There are three methodological limitations that should be considered. To begin with, the use of optical NDVI adds the vulnerability to cloud contamination and atmospheric scattering - especially in tropical volcanoes where cloudiness is persistent. Moreover, saturation of NDVI in high-biomass canopies (usually at values around 0.80-0.85) limits the sensitivity of the index to structural development during late-successional stages of forest. Additional indices (EVI or EVI2) that have lower saturation during dense canopy conditions (Jiang *et al*., 2008; Huete *et al*., 2002; Didan, 2015) are suggested to solve recovery dynamics in late succession stages. Second, the lack of in-situ data on the species composition, above-ground biomass, and canopy structure limits the ecological explanation of the NDVI trajectory. The NDVI overshoot associated with pioneer community proliferation has been observed at Mount Kelud post-eruption, and with similar overshoot patterns observed in post-disturbance recovery studies at subtropical and tropical volcanoes (Del Moral *et al*., 2003; Del Moral *et al*., 1995; Kuenzer *et al*., 2015). Third, the 100-point sample network, however spread out spatially over the eruption-affected flanks, can sample the proximal summit zone, in which pyroclastic and ballistic impacts were most localized, and heterogeneity of disturbances is the highest.

Despite such restrictions, the current research contains evidence-based quantification of post-eruption vegetation recovery in Mount Kelud that has direct application to risk of hazards-related assessment, land management, and monitoring program design in active Indonesian volcanoes. The recorded recovery rate implies that, with no repeat large events or systematic anthropogenic land habitats, the volcano flanks could achieve a structurally mature secondary forest stage within a period significantly shorter in comparison to those recorded in similar volcanic disturbances in temperate and non-tropical Asian surroundings. This result is in line with the established sensitivity of tropical ecosystems to rapid pioneer-stage succession following volcanic perturbation (Tsuyuzaki & Hase, 2005; Zobel & Antos, 2009; Chang *et al*., 2019; Biass *et al*., 2022

4. CONCLUSION

In this study, the temporal and spatial dynamics of vegetation recovery after the eruption at Mount Kelud were quantified using multi-sensor NDVI data of Landsat 8 and Sentinel-2 data on the same parameter between 2013 and 2025. The February 2014 eruption caused a substantial decline in vegetation condition, with NDVI decreasing by more than 0.50 units from pre-eruption levels (0.75-0.88). Irrespective of this disruption, the recovery of vegetation was fast, and NDVI went back to the pre-disturbance level in around one year and even higher in the following years (above the baseline (0.80-0.87)). The damage evaluation showed that there was mostly low-severity disturbance (89% of locations), which was a manifestation of spatial heterogeneity in eruption effects. Statistical analysis also confirmed that seasonal variations

did not play any significant role in NDVI dynamics ($r = 0.095$, $p > 0.05$), and thus, vegetation change was predominantly influenced by the disturbance instead of the seasonality of climatic factors. The findings indicate the high resilience of tropical volcanic ecosystems and show that a combination of multi-sensor remote sensing data provides effective long-term monitoring of the environment. Further research is needed to provide field-based validation and other spectral indices to enhance the precision of vegetation recovery measurement approaches for long-term environmental surveillance.

5. ACKNOWLEDGEMENTS

The authors acknowledged the United States Geological Survey (USGS) and the European Space Agency (ESA) for providing open-access satellite data used in this study.

REFERENCES

Arjasakusuma, S., Khoirurrizqi, Y., & Huwaida, T. (2025). Assessing the coherency of different El Niño events with vegetation health using time-series remote sensing data and wavelet coherency analysis in part of Southeast Asia. *Remote Sensing Applications: Society and Environment*, *37*, 101460. https://doi.org/10.1016/j.rsase.2025.101460

Berveglieri, A., Imai, N. N., Christovam, L. E., Galo, M. L. B. T., Tommaselli, A. M. G., & Honkavaara, E. (2021). Analysis of trends and changes in the successional trajectories of tropical forest using the Landsat NDVI time series. *Remote Sensing Applications: Society and Environment*, *24*, 100622. https://doi.org/10.1016/j.rsase.2021.100622

Biass, S., Jenkins, S. F., Aeberhard, W. H., Delmelle, P., & Wilson, T. (2022). Insights into the vulnerability of vegetation to tephra fallouts from interpretable machine learning and big Earth observation data. *Natural Hazards and Earth System Sciences*, *22*(9), 2829–2855. https://doi.org/10.5194/nhess-22-2829-2022

Black, B. A., Griffin, D., Van Der Sleen, P., Wanamaker, A. D., Speer, J. H., Frank, D. C., Stahle, D. W., Pederson, N., Copenheaver, C. A., Trouet, V., Griffin, S., & Gillanders, B. M. (2016). The value of crossdating to retain high-frequency variability, climate signals, and extreme events in environmental proxies. *Global Change Biology*, *22*(7), 2582–2595. https://doi.org/10.1111/gcb.13256

Cardille, J. A., Perez, E., Crowley, M. A., Wulder, M. A., White, J. C., & Hermosilla, T. (2022). Multi-sensor change detection for within-year capture and labelling of forest disturbance. *Remote Sensing of Environment*, *268*, 112741. https://doi.org/10.1016/j.rse.2021.112741

Chang, C. C., Halpern, C. B., Antos, J. A., Avolio, M. L., Biswas, A., Cook, J. E., Del Moral, R., Fischer, D. G., Holz, A., Pabst, R. J., Swanson, M. E., & Zobel, D. B. (2019). Testing conceptual models of early plant succession across a disturbance gradient. *Journal of Ecology*, *107*(2), 517–530. https://doi.org/10.1111/1365-2745.13120

Chen, C., Park, T., Wang, X., Piao, S., Xu, B., Chaturvedi, R. K., Fuchs, R., Brovkin, V., Ciais, P., Fensholt, R., Tømmervik, H., Bala, G., Zhu, Z., Nemani, R. R., & Myneni, R. B. (2019). China and India lead in greening of the world through land-use management. *Nature Sustainability*, *2*(2), 122–129. https://doi.org/10.1038/s41893-019-0220-7

Chen, Y., Cao, R., Liu, S., Peng, L., Chen, X., & Chen, J. (2024). A new deep learning-based model for reconstructing high-quality NDVI time-series data in heavily cloudy areas: Fusion of Sentinel 1 and 2 data. *International Journal of Digital Earth*, *17*(1), e2407941. https://doi.org/10.1080/17538947.2024.2407941

Chiessi, V., D'Orefice, M., Scarascia Mugnozza, G., Vitale, V., & Cannese, C. (2010). Geological, geomechanical and geostatistical assessment of rockfall hazard in San Quirico Village (Abruzzo, Italy). *Geomorphology*, *119*(3–4), 147–161. https://doi.org/10.1016/j.geomorph.2010.03.010

Chilton, K. D., & Spotila, J. A. (2020). Preservation of Valley and Ridge topography via delivery of resistant, ridge-sourced boulders to hillslopes and channels, Southern Appalachian Mountains, U.S.A. *Geomorphology*, *365*, 107263. https://doi.org/10.1016/j.geomorph.2020.107263

Claverie, M., Ju, J., Masek, J. G., Dungan, J. L., Vermote, E. F., Roger, J.-C., Skakun, S. V., & Justice, C. (2018). The Harmonized Landsat and Sentinel-2 surface reflectance data set. *Remote Sensing of Environment*, *219*, 145–161. https://doi.org/10.1016/j.rse.2018.09.002

Dahlgren, R. A., Saigusa, M., & Ugolini, F. C. (2004). The Nature, Properties and Management of Volcanic Soils. In *Advances in Agronomy* (Vol. 82, pp. 113–182). Elsevier. https://doi.org/10.1016/S0065-2113(03)82003-5

Del Moral, R., Titus, J. H., & Cook, A. M. (1995). Early primary succession on Mount St. Helens, Washington, USA. *Journal of Vegetation Science*, *6*(1), 107–120. https://doi.org/10.2307/3236262

Didan, K. (2015). *MOD13Q1 MODIS/Terra Vegetation Indices 16-Day L3 Global 250m SIN Grid V006* [Dataset]. NASA Land Processes Distributed Active Archive Center. https://doi.org/10.5067/MODIS/MOD13Q1.006

Furusawa, T., Koera, T., Siburian, R., Wicaksono, A., Matsudaira, K., & Ishioka, Y. (2023a). Time-series analysis of satellite imagery for detecting vegetation cover changes in Indonesia. *Scientific Reports*, *13*(1), 8437. https://doi.org/10.1038/s41598-023-35330-1

Furusawa, T., Koera, T., Siburian, R., Wicaksono, A., Matsudaira, K., & Ishioka, Y. (2023b). Time-series analysis of satellite imagery for detecting vegetation cover changes in Indonesia. *Scientific Reports*, *13*(1), 8437. https://doi.org/10.1038/s41598-023-35330-1

Gao, S., Zhong, R., Yan, K., Ma, X., Chen, X., Pu, J., Gao, S., Qi, J., Yin, G., & Myneni, R. B. (2023). Evaluating the saturation effect of vegetation indices in forests using 3D radiative transfer simulations and satellite observations. *Remote Sensing of Environment*, *295*, 113665. https://doi.org/10.1016/j.rse.2023.113665

Gao, X. (2000). Optical–Biophysical Relationships of Vegetation Spectra without Background Contamination. *Remote Sensing of Environment*, *74*(3), 609–620. https://doi.org/10.1016/S0034-4257(00)00150-4

Geertsema, M., & Pojar, J. J. (2007). Influence of landslides on biophysical diversity—A perspective from British Columbia. *Geomorphology*, *89*(1–2), 55–69. https://doi.org/10.1016/j.geomorph.2006.07.019

Global Volcanism Program. (2014). Report on Kelut (Indonesia). *Bulletin of the Global Volcanism Network*, *39*(2). https://doi.org/10.5479/si.GVP.BGVN201402-263280

Huang, S., Tang, L., Hupy, J. P., Wang, Y., & Shao, G. (2021). A commentary review on the use of normalized difference vegetation index (NDVI) in the era of popular remote sensing. *Journal of Forestry Research*, *32*(1), 1–6. https://doi.org/10.1007/s11676-020-01155-1

Huete, A., Didan, K., Miura, T., Rodriguez, E. P., Gao, X., & Ferreira, L. G. (2002a). Overview of the radiometric and biophysical performance of the MODIS vegetation indices. *Remote Sensing of Environment*, *83*(1–2), 195–213. https://doi.org/10.1016/S0034-4257(02)00096-2

Huete, A., Didan, K., Miura, T., Rodriguez, E. P., Gao, X., & Ferreira, L. G. (2002b). Overview of the radiometric and biophysical performance of the MODIS vegetation indices. *Remote Sensing of Environment*, *83*(1–2), 195–213. https://doi.org/10.1016/S0034-4257(02)00096-2

Ichii, K., Kawabata, A., & Yamaguchi, Y. (2002). Global correlation analysis for NDVI and climatic variables and NDVI trends: 1982-1990. *International Journal of Remote Sensing*, *23*(18), 3873–3878. https://doi.org/10.1080/01431160110119416

Ishaq, R. M., Hairiah, K., Alfian, I., & Van Noordwijk, M. (2020). Natural Regeneration After Volcanic Eruptions: Resilience of the Non-legume Nitrogen-Fixing Tree Parasponia rigida. *Frontiers in Forests and Global Change*, *3*, 562303. https://doi.org/10.3389/ffgc.2020.562303

Jiang, Z., Huete, A., Didan, K., & Miura, T. (2008). Development of a two-band enhanced vegetation index without a blue band. *Remote Sensing of Environment*, *112*(10), 3833–3845. https://doi.org/10.1016/j.rse.2008.06.006

Jin, J., Jian, D., Zhou, X., Chen, Q., & Li, Y. (2025). Impact of El Niño–Southern Oscillation on Global Vegetation. *Atmosphere*, *16*(6), 701. https://doi.org/10.3390/atmos16060701

Kong, K., Deng, Z., Chen, F., Wang, Z., & Chen, Y. (2025). Numerical analysis of the effect of vegetation root reinforcement on the rainfall-induced instability of loess slopes. *Scientific Reports*, *15*(1), 23233. https://doi.org/10.1038/s41598-025-06400-3

Kuenzer, C., Dech, S., & Wagner, W. (Eds.). (2015). *Remote Sensing Time Series: Revealing Land Surface Dynamics* (Vol. 22). Springer International Publishing. https://doi.org/10.1007/978-3-319-15967-6

Lai, R., Oguchi, T., & Zhong, C. (2022). Evaluating Spatiotemporal Patterns of Post-Eruption Vegetation Recovery at Unzen Volcano, Japan, from Landsat Time Series. *Remote Sensing*, *14*(21), 5419. https://doi.org/10.3390/rs14215419

Lancheros, J. C., Madera-Parra, C. A., Caselles-Osorio, A., Torres-López, W. A., & Vargas-Ramírez, X. M. (2019). Ibuprofen and Naproxen removal from domestic wastewater using a Horizontal Subsurface Flow Constructed Wetland coupled to Ozonation. *Ecological Engineering*, *135*, 89–97. https://doi.org/10.1016/j.ecoleng.2019.05.007

Lusiana, N., Adliya, G. E., Devianto, L. A., & Husin, N. A. (2026). Rapid post-landslide vegetation regrowth detected by multi-temporal satellite imagery in the Southern part

of Mt. Rinjani National Park, Lombok, Indonesia. *Natural Hazards*, *122*(5), 191. https://doi.org/10.1007/s11069-025-07964-z

Maeno, F., Nakada, S., Yoshimoto, M., Shimano, T., Hokanishi, N., Zaennudin, A., & Iguchi, M. (2019). A sequence of a plinian eruption preceded by dome destruction at Kelud volcano, Indonesia, on February 13, 2014, revealed from tephra fallout and pyroclastic density current deposits. *Journal of Volcanology and Geothermal Research*, *382*, 24–41. https://doi.org/10.1016/j.jvolgeores.2017.03.002

Mandl, L., Stritih, A., Seidl, R., & Senf, C. (2026). The role of thermal constraints in post-disturbance forest recovery across the European Alps – a large-scale remote sensing study. *Agricultural and Forest Meteorology*, *378*, 111016. https://doi.org/10.1016/j.agrformet.2026.111016

McLean, K. I., Mushet, D. M., Newton, W. E., & Sweetman, J. N. (2021). Long-term multidecadal data from a prairie-pothole wetland complex reveal controls on aquatic-macroinvertebrate communities. *Ecological Indicators*, *126*, 107678. https://doi.org/10.1016/j.ecolind.2021.107678

Nagai, S., Ichii, K., & Morimoto, H. (2007). Interannual variations in vegetation activities and climate variability caused by ENSO in tropical rainforests. *International Journal of Remote Sensing*, *28*(6), 1285–1297. https://doi.org/10.1080/01431160600904972

Nguyen, T. H., Jones, S. D., Soto-Berelov, M., Haywood, A., & Hislop, S. (2018). A spatial and temporal analysis of forest dynamics using Landsat time-series. *Remote Sensing of Environment*, *217*, 461–475. https://doi.org/10.1016/j.rse.2018.08.028

Patera, V., Di Fazio, S., Messina, G., & Praticò, S. (2026). The Application of Remote Sensing Technologies in Pastures Monitoring: A Review for the Mediterranean Region. *Sustainability*, *18*(3), 1642. https://doi.org/10.3390/su18031642

Plank, S., Twele, A., & Martinis, S. (2016). Landslide Mapping in Vegetated Areas Using Change Detection Based on Optical and Polarimetric SAR Data. *Remote Sensing*, *8*(4), 307. https://doi.org/10.3390/rs8040307

Poorter, L., Bongers, F., Aide, T. M., Almeyda Zambrano, A. M., Balvanera, P., Becknell, J. M., Boukili, V., Brancalion, P. H. S., Broadbent, E. N., Chazdon, R. L., Craven, D., De Almeida-Cortez, J. S., Cabral, G. A. L., De Jong, B. H. J., Denslow, J. S., Dent, D. H., DeWalt, S. J., Dupuy, J. M., Durán, S. M., … Rozendaal, D. M. A. (2016a). Biomass resilience of Neotropical secondary forests. *Nature*, *530*(7589), 211–214. https://doi.org/10.1038/nature16512

Poorter, L., Bongers, F., Aide, T. M., Almeyda Zambrano, A. M., Balvanera, P., Becknell, J. M., Boukili, V., Brancalion, P. H. S., Broadbent, E. N., Chazdon, R. L., Craven, D., De Almeida-Cortez, J. S., Cabral, G. A. L., De Jong, B. H. J., Denslow, J. S., Dent, D. H., DeWalt, S. J., Dupuy, J. M., Durán, S. M., … Rozendaal, D. M. A. (2016b). Biomass resilience of Neotropical secondary forests. *Nature*, *530*(7589), 211–214. https://doi.org/10.1038/nature16512

Qian, X., Qiu, B., & Zhang, Y. (2019). Widespread Decline in Vegetation Photosynthesis in Southeast Asia Due to the Prolonged Drought During the 2015/2016 El Niño. *Remote Sensing*, *11*(8), 910. https://doi.org/10.3390/rs11080910

Rösch, M., & Plank, S. (2022). Detailed Mapping of Lava and Ash Deposits at Indonesian Volcanoes by Means of VHR PlanetScope Change Detection. *Remote Sensing*, *14*(5), 1168. https://doi.org/10.3390/rs14051168

Saito, H., Uchiyama, S., & Teshirogi, K. (2022a). Rapid vegetation recovery at landslide scars detected by multitemporal high-resolution satellite imagery at Aso volcano, Japan. *Geomorphology*, *398*, 107989. https://doi.org/10.1016/j.geomorph.2021.107989

Saito, H., Uchiyama, S., & Teshirogi, K. (2022b). Rapid vegetation recovery at landslide scars detected by multitemporal high-resolution satellite imagery at Aso volcano, Japan. *Geomorphology*, *398*, 107989. https://doi.org/10.1016/j.geomorph.2021.107989

Shin, N., Katsumata, C., Miura, T., Tsutsumida, N., Ichie, T., Kotani, A., Nakagawa, M., Khoon, K. L., Kobayashi, H., Kumagai, T., Tei, S., Pungga, R. A. S., Yamada, T., Kameda, A., Yanagisawa, M., Nasahara, K. N., Muraoka, H., Ichii, K., & Tokumoto, Y. (2023). Perspective: Improving the accuracy of plant phenology observations and land-cover and land-use detection by optical satellite remote-sensing in the Asian tropics. *Frontiers in Forests and Global Change*, *6*, 1106723. https://doi.org/10.3389/ffgc.2023.1106723

Song, X., Tan, Y., & Lu, Y. (2024). Microscopic analyses of the reinforcement mechanism of plant roots in different morphologies on the stability of soil slopes under heavy rainfall. *CATENA*, *241*, 108018. https://doi.org/10.1016/j.catena.2024.108018

Sundha, P., Basak, N., Rai, A. K., Yadav, R. K., Sharma, P. C., & Sharma, D. K. (2020). Can conjunctive use of gypsum, city waste composts and marginal quality water rehabilitate saline-sodic soils? *Soil and Tillage Research*, *200*, 104608. https://doi.org/10.1016/j.still.2020.104608

Suzuki, Y. J., & Iguchi, M. (2019). Determination of the mass eruption rate for the 2014 Mount Kelud eruption using three-dimensional numerical simulations of volcanic plumes. *Journal of Volcanology and Geothermal Research*, *382*, 42–49. https://doi.org/10.1016/j.jvolgeores.2017.06.011

Tsuyuzaki, S., & Hase, A. (2005). Plant community dynamics on the volcano Mount Koma, northern Japan, after the 1996 eruption. *Folia Geobotanica*, *40*(4), 319–330. https://doi.org/10.1007/BF02804282

Tucker, C. J. (1979a). Red and photographic infrared linear combinations for monitoring vegetation. *Remote Sensing of Environment*, *8*(2), 127–150. https://doi.org/10.1016/0034-4257(79)90013-0

Tucker, C. J. (1979b). Red and photographic infrared linear combinations for monitoring vegetation. *Remote Sensing of Environment*, *8*(2), 127–150. https://doi.org/10.1016/0034-4257(79)90013-0

Verbesselt, J., Hyndman, R., Newnham, G., & Culvenor, D. (2010). Detecting trend and seasonal changes in satellite image time series. *Remote Sensing of Environment*, *114*(1), 106–115. https://doi.org/10.1016/j.rse.2009.08.014

Verbesselt, J., Hyndman, R., Zeileis, A., & Culvenor, D. (2010). Phenological change detection while accounting for abrupt and gradual trends in satellite image time series. *Remote Sensing of Environment*, *114*(12), 2970–2980. https://doi.org/10.1016/j.rse.2010.08.003

Walker, L. R., & Del Moral, R. (2003). *Primary Succession and Ecosystem Rehabilitation* (1st ed.). Cambridge University Press. https://doi.org/10.1017/CBO9780511615078

Wu, C.-H. (2021a). Evaluating the Landslide Stability and Vegetation Recovery: Case Studies in the Tsengwen Reservoir Watershed in Taiwan. *Water*, *13*(24), 3479. https://doi.org/10.3390/w13243479

Wu, C.-H. (2021b). Evaluating the Landslide Stability and Vegetation Recovery: Case Studies in the Tsengwen Reservoir Watershed in Taiwan. *Water*, *13*(24), 3479. https://doi.org/10.3390/w13243479

Wulder, M. A., Roy, D. P., Radeloff, V. C., Loveland, T. R., Anderson, M. C., Johnson, D. M., Healey, S., Zhu, Z., Scambos, T. A., Pahlevan, N., Hansen, M., Gorelick, N., Crawford, C. J., Masek, J. G., Hermosilla, T., White, J. C., Belward, A. S., Schaaf, C., Woodcock, C. E., … Cook, B. D. (2022). Fifty years of Landsat science and impacts. *Remote Sensing of Environment*, *280*, 113195. https://doi.org/10.1016/j.rse.2022.113195

Zhang, Y., Zhu, Z., Liu, Z., Zeng, Z., Ciais, P., Huang, M., Liu, Y., & Piao, S. (2016). Seasonal and interannual changes in vegetation activity of tropical forests in Southeast Asia. *Agricultural and Forest Meteorology*, *224*, 1–10. https://doi.org/10.1016/j.agrformet.2016.04.009

Zheng, L., Li, L., Chen, Z., He, Y., Mo, L., Chen, D., Hu, Q., Wang, L., Liang, Q., & Cheng, X. (2023). Multi-sensor imaging of winter buried lakes in the Greenland Ice Sheet. *Remote Sensing of Environment*, *295*, 113688. https://doi.org/10.1016/j.rse.2023.113688

Zhong, C., Li, C., Gao, P., & Li, H. (2021). Discovering Vegetation Recovery and Landslide Activities in the Wenchuan Earthquake Area with Landsat Imagery. *Sensors*, *21*(15), 5243. https://doi.org/10.3390/s21155243

Zhu, Z., Piao, S., Myneni, R. B., Huang, M., Zeng, Z., Canadell, J. G., Ciais, P., Sitch, S., Friedlingstein, P., Arneth, A., Cao, C., Cheng, L., Kato, E., Koven, C., Li, Y., Lian, X., Liu, Y., Liu, R., Mao, J., … Zeng, N. (2016). Greening of the Earth and its drivers. *Nature Climate Change*, *6*(8), 791–795. https://doi.org/10.1038/nclimate3004

Zobel, D. B., & Antos, J. A. (2009). Species properties and recovery from disturbance: Forest herbs buried by volcanic tephra. *Journal of Vegetation Science*, *20*(4), 650–662. https://doi.org/10.1111/j.1654-1103.2009.01057.x